Atmos. Chem. Phys. Discuss., 6, 1023–1071, 2006
www.atmos-chem-phys.org/acpd/6/1023/
SRef-ID: 1680-7375/acpd/2006-6-1023
European Geosciences Union

Atmospheric Chemistry and Physics Discussions

Impact of ship emissions on the microphysical, optical and radiative properties of marine stratus: a case study

M. Schreier[1], A. A. Kokhanovsky[1], V. Eyring[2], L. Bugliaro[2], H. Mannstein[2], B. Mayer[2], H. Bovensmann[1], and J. P. Burrows[1]

[1]Institute for Environmental Physics (IUP), University of Bremen, Germany
[2]Institut für Physik der Atmosphäre, DLR-Oberpfaffenhofen, Wessling, Germany

Received: 29 November 2005 – Accepted: 10 December 2005 – Published: 3 February 2006

Correspondence to: M. Schreier (schreier@iup.physik.uni-bremen.de)

Abstract

Modifications of existing clouds by the exhaust of ships are well-known but poorly studied atmospheric effects which could contribute to climate change. The perturbation of a cloud layer by ship-generated aerosol changes the cloud reflectivity and is identified by long curves in satellite images, known as ship tracks. As ship tracks indicate a pollution of a very clean marine environment and also affect the radiation budget below and above the cloud, it is important to investigate their radiative and climatic effects. Satellite-data from MODIS on Terra are used to examine a scene from 10 February 2003 where ship tracks were detected close to the North American West-Coast. The cloud optical and microphysical properties are derived using a semi-analytical retrieval technique combined with a look-up-table approach. Ship-track-pixels are distinguished from the unperturbed cloud pixels and the optical properties of the former are compared to those of the latter. Within the ship tracks a significant change in the droplet number concentration, the effective radius and the optical thickness are found compared to the unaffected cloud. Significant increase of liquid water could not be confirmed. The resulting cloud properties are used to calculate the radiation budget below and above the cloud. Assuming a mean solar zenith angle, the mean surface radiation below the ship track is decreased by 43.25 Wm^{-2} and the mean reflectance at TOA is increased by 40.73 Wm^{-2}. For the selected scene the ship emission decreases the solar radiation at the surface by 2.10 Wm^{-2} and increases the backscattered solar radiation at top of the atmosphere (TOA) by 2.00 Wm^{-2}. Increased backscattered radiation is partly compensated by a decrease of the thermal radiation of 0.43 Wm^{-2}. The resulting net-effect at TOA is an increase of 1.57 Wm^{-2} corresponding to a negative radiative forcing and a cooling.

ACPD

6, 1023–1071, 2006

1. Introduction

Emissions by ships significantly contribute to the total budget of anthropogenic emissions. The exhaust gas emissions from ships include CO_2, NO_x, SO_x, CO, hydrocarbons, and particulate matter (Eyring et al., 2005a). Recently, satellite measurements of NO_2 showed enhanced NO_2 column amounts along major international shipping routes (Richter et al., 2004; Beirle et al., 2005). Ship emissions are released into the marine boundary layer and change the chemical composition of the atmosphere (Lawrence et al., 1999; Kasibhatla et al., 2000; Davis et al., 2001; Endresen et al., 2003) and climate (Capaldo et al., 1999; Endresen et al., 2003). Compared to other transport modes, the sulphur content of the fuel burned in marine diesel engines and the total amount of SO_x emissions is high (Eyring et al., 2005a). The average sulphur fuel content of today's world-merchant shipping fleet is 2.4% that results in a large amount of SO_2 and particulate matter emissions (EPA, 2000). International maritime conventions do not regulate the sulphur content of fuel for shipping. However, there are regional and local emission legislations, for NO_x but also for SO_x and particulate matter (Entec, 2002; World Bunkering, 2004). During the last 50 years, the world's ocean-going fleet and the ships' total fuel consumption have increased considerably. Further increase of fuel consumption and emissions is expected in the future related to an increase in economic growth and sea borne trade (Eyring et al., 2005a, b). Ship emissions have been recognized as a growing problem by both policy makers and scientists (Corbett, 2003).

In addition to the impact on tropospheric chemistry, particle emissions from ships also change the physical properties of low clouds. This is the so-called indirect aerosol-effect, which has been observed in satellite data in many studies (e.g., Conover, 1966; Twomey et al., 1968; Radke et al., 1989). One important factor contributing to the indirect aerosol effect is sulphur emissions by shipping.

The expected increase of emissions makes it important to examine the effects of global ship traffic on the climate system. Cloud modification by ship aerosol emissions

ACPD
6, 1023–1071, 2006

is an important effect because clouds are regulators of the climate system. Natural aerosol in a maritime environment consists of a small amount of particles mainly composed of sea salt with diameters greater than 1 μm (O'Dowd et al., 1997, 2004) and sulphate particles with diameters less than 1 μm (McInnes et al., 1996). The low number of particles results in small optical thickness (Christopher and Zhang, 2002) and a small amount of aerosol available for cloud condensation. This limited number of cloud condensation nuclei is reflected in larger droplets and a smaller droplet number concentration in low-level stratiform clouds over the ocean compared to continental clouds (Miles et al., 2000). If additional aerosols are injected, the changes of the aerosol concentration and amount result in a change in the droplet number concentration within the cloud (Facchini et al., 1999), depending on the solubility and size of the injected aerosol particles. Particles and their precursors from ship emissions are able to act as cloud condensation nuclei (CCN) in the water-vapour saturated environment of the maritime cloud or can change the surface tension due to the solubility. Which particulate matter of ship emissions is able to act as CCN is not entirely clarified, but especially the high sulphur content of the fuel may be an important factor for the modification of clouds, because the resulting SO_x is able to act as CCN (Seinfeld and Pandis, 1997). Amount and size of these particles depends on the fuel and also the kind of combustion, but can possibly result in a higher droplet concentration (Twomey et al., 1968; Twomey, 1974) and consequently in a change of reflectivity of the maritime cloud.

Measurements in the Monterey Ship Track Experiment confirm this hypothesis (Durkee et al., 2000a). In the plumes, Hobbs et al. (2000) observed an increased amount of those particles which can act as CCNs in a supersaturated environment as well as the related increase in the cloud droplet concentration and the decrease in the cloud effective radius. Slight changes in the particle size distribution were reported by Öström et al. (2000). On the other hand, there was no evidence for the influence of sea salt particles (Durkee et al., 2000b) from the wake of the ship on the clouds and also no significant influence of heat and moisture from the ship stack (Hobbs et al., 2000). So, these measurements confirm the role of emitted particles as CCNs and especially the

importance of SO_x.

Also further effects of aerosols on clouds are suggested. Albrecht (1989) proposed possible drizzle suppression due to the increase of CCN resulting in a higher amount of liquid water in the cloud whereas Han et al. (2002) estimate a possible decrease of liquid water in the cloud. Ferek et al. (2000) showed by measurements slight indications for increased liquid water in the cloud and possible drizzle suppression.

Modifications of clouds by aerosols result in a significantly higher droplet concentration. This leads to an increased scattering, resulting in larger reflectances. This increased reflectance however, might be partially reduced due to the presence of highly absorbing particles (e.g. soot) in the plume exhaust. The increased reflectivity is even higher in the near infrared, because here, the ratio of absorption to scattering is strongly depending on the droplet size (Kokhanovsky et al., 2004a).

In this study the modification of clouds and the influence of the ship exhaust on the radiation budget of a given scene is examined. Satellite data are used to retrieve cloud properties and their modifications due to ship emissions. Section 2 gives an overview of the selected satellite scene. Section 3 explains the approach for extracting the polluted (ship track) pixels and the algorithms to analyze microphysical and optical properties of the cloud. They are based on the semi-analytical cloud retrieval algorithm SACURA (Kokhanovsky et al., 2003) combined with look-up-tables for thin clouds calculated with the libRadtran radiative transfer package (Mayer and Kylling, 2005). The work concentrates on low clouds because only those are affected by ship emissions. The section is also addressed to the question how foam and turbulent waves caused in the ship wake may affect the reflectances and hence the derived cloud properties. The last part of this section describes calculations to determine the impact on the radiation budget.

The results of this study are presented in Sect. 4. The cloud mask separating track-pixels and no-track-pixels is shown in Sect. 4.1. Changes in the effective radius, optical thickness, liquid water path, and droplet number concentration due to the exhaust plume are presented in Sect. 4.2. The resulting optical parameters obtained from the

ACPD
6, 1023–1071, 2006

image analysis are used in Sect. 4.3 to calculate the radiation below and above the cloud and to estimate the influence of the modified clouds on the radiation close to the surface and also at the top of the atmosphere. Also possible drizzle suppression is discussed in this section.

2. Selected ship track scene

For our analysis a particular and adequate satellite scene from Terra-MODIS (King et al., 1995) was selected. The scene from 10 February 2003, close to the West Coast of North America (153° W to 120° W and 40° N to 60° N), exhibits a number of anomalous cloud lines in the stratiform clouds over the ocean. Figure 1 shows the reflectance in MODIS-data for channel 2 (0.85 μm) and Fig. 2 the reflectance for channel 7 (2.13 μm). These two channels are also used for the ship track detection. As explained above, the curves are more pronounced in the 2.13 μm-channel. The time of the satellite overpass is 20:25 UTC (11:25 local time) the solar zenith angle is between 55° and 79°, depending on the location in the image. The observed cloud seems to be a typical formation for this time of the day over the Northern Pacific (Norris, 1998a, b; Whang et al., 2000).

The scene contains the Northern Pacific and on the eastern edge, the American coast is visible. Large ports like Vancouver and Seattle (see Fig. 1) are located on this coastline. A comparison with 1×1 degree vessel traffic density for the year 2000 (Endresen et al., 2003) for the area (Fig. 3) shows high density of ship traffic for the domain of the satellite scene. Any impact of air traffic is eliminated by taking into account the brightness temperature of the clouds, using the MODIS atmospheric window channel 31 (11 μm, Fig. 4). The temperatures indicate low warm clouds for the anomalous cloud lines and therefore the impact of aircraft emissions is negligible. Meteorological conditions taken from ECMWF reanalysis data (ERA-40-project, Simmons and Gibson, 2001) for a geopotential height of 700 m above the ocean show a high pressure field over the northern Pacific with an anticyclonic wind field (Fig. 5). The curves are con-

ACPD
6, 1023–1071, 2006

sistent with ship-traffic coming from or going to the great harbours of the West coast of North America being turned by the wind field. In conclusion it is very unlikely that this anomalous cloud lines have a source other than ship traffic emissions.

3. Methods

An automatic algorithm to detect ship tracks has been developed in order to study how ship emissions modify clouds. Figure 6 shows a flow diagram of the ship track algorithm. The algorithm distinguishes between track-pixels and no-track-pixels, that is, polluted and unpolluted pixels. In addition, optical and physical properties of the low clouds are calculated and the derived optical properties are used to estimate the influence on the radiation budget.

3.1. Ship track mask algorithm

The upper part of the flow diagram in Fig. 6 shows the criteria that are used to identify ship-track-pixels. Sea pixels are first separated from land pixels by means of a land-sea-mask. Then a filter is applied to extract only those cloudy pixels, which are susceptible for the exhaust of ships. To determine a threshold for cloudy pixels, histogram analysis of the reflectance was performed. For a pixel to be classified as cloudy, its reflectance at 650 nm (Channel 1) has to be higher than $R_{threshhold}$=0.1. Ship emissions can only modify low stratiform clouds over the ocean, when the cloud top height is below approximately 1500 m (Durkee et al., 2000b). Taking into account the temperature of the ocean and a lapse rate for a wet-adiabatic environment like the maritime boundary layer, the cloud top height can be estimated from the brightness temperature in channel 31 (11 μm). To separate low cloud pixels from cloudy pixels the temperature difference ΔT between the sea surface temperature (T_{ocean}) and the temperature of the cloudy pixels must be smaller than 10.5 K. The sea surface temperature T_{ocean} is taken from nearby cloud free pixels, while ΔT has been calculated assuming a wet-adiabatic

ACPD
6, 1023–1071, 2006

lapse rate of 0.7 K/100 m for the maritime boundary layer and a maximum top altitude of 1500 m. The temperature criterion also excludes the detection of aircraft contrails, as the algorithm only detects warm clouds. The remaining cloud covered pixels were classified as low-cloud-pixel.

In a last step, pattern recognition, in particular edge filtering, was used in order to identify changes in the cloud reflectance, which indicate ship tracks. Enhancement of the edges was achieved by dividing the values of the satellite data from channel 2 (0.85 μm) and channel 7 (2.13 μm). Channel 7 is a good indicator for cloud modifications and therefore ship tracks, because the reflectivity strongly depends on the ratio of absorption to scattering in the near infrared, which can be seen in Fig. 2. Channel 2 helps to increase contrast for pixels with increased scattering. Using both channels, the contrast for pixels with a significant influence on the radiation, is increased.

The edge filtering does not distinguish between ship-track-pixels and natural edges. To select the ship track relevant pixels automatically the following criteria were applied in addition:

- The number of pixels between two edge-pixels should not exceed a threshold, chosen for narrow curves;
- The length and width of connected pixel-clusters should not exceed a threshold;
- The number of neighbouring and connected pixels in an area should not exceed a threshold.

The thresholds were optimized manually to minimize the false detection of clouds, by excluding edges that are obviously not ship tracks but natural cloud formation edges. The result is a differentiation of the low-cloud-pixels divided into the two categories ship-track-pixels and no-ship-track-pixels.

ACPD
6, 1023–1071, 2006

3.2. Cloud properties retrieval

The optical and microphysical parameters of the cloud were derived from channel 2 (0.85 μm) and channel 6 (1.6 μm). 1.6 μm was selected because the smaller absorption of liquid water enables more accurate results for the retrievals. The used algorithms were SACURA (Kokhanovsky et al., 2003), a fast semi-analytical approach, and for optically thin clouds a look-up-table (LUT) approach based on the radiative transfer code libRadtran (Mayer and Kylling, 2005). The approaches are different, but both derive the cloud optical thickness and also the effective radius r_{eff}, defined by the ratio of the third to second moment of the particle size distribution and therefore indicating a change of the ratio of volume to surface in the particle size distribution.

SACURA is a semi-analytical approach based on the fact that the probability of photon absorption by droplets in the visible and near-infrared spectral regions is low (Kokhanovsky et al., 2003). The technique relies upon asymptotic equations of the radiative transfer theory valid for the values of the single scattering albedo ω_0 close to one, which allows a much faster calculation of reflectances than a numerical solution of the radiative transfer equation. SACURA was compared to other cloud retrieval algorithms (Nauss et al., 2005) and the retrieved values agreed well. SACURA calculates the effective radius from the observed reflectances and uses this value to derive optical thickness and liquid water path, assuming a vertically homogeneous cloud. The ocean surface reflectance for SACURA was assumed to be 0.03 for 0.85 μm and 0.0 for 1.6 μm. The advantages of SACURA are its speed and high accuracy and also an interpolation is not necessary. A disadvantage of SACURA is the increasing error for decreasing cloud optical thickness.

Therefore, for clouds with an optical thickness of 5 and below, a look-up-table approach and an interpolation is used, to have a wider range of applicability in terms of the cloud optical thickness. The look-up-table (LUT) is calculated using the radiative transfer code libRadtran (Mayer and Kylling, 2005), assuming mid-latitude standard atmosphere and a cloud top height of 1000 m. The scattering properties of the cloud are

ACPD
6, 1023–1071, 2006

based on Mie-calculations and the assumed surface reflectance was the same as for SACURA. Reflectances were calculated for a wide range of optical thicknesses and effective radii. A best-fit method is used to find the cloud optical thickness and r_{eff} for the observed reflectances. The liquid water path in the LUT is calculated via cloud optical thickness and r_{eff} assuming a vertically homogeneous cloud.

The droplet number concentration for both retrievals is calculated via effective radius and cloud optical thickness by assuming a gamma droplet size distribution with a coefficient of variance of 0.37 as proposed by Deirmendjian (1969). Calculations were performed for a hypothetical vertical homogeneous cloud of a thickness of 500 m, which is a reasonable value for low marine stratiform clouds (Cahalan et al., 1994; Han et al., 1998). The value of thickness is not important for the relative changes of the droplet spectra but resulting values per volume are useful for comparing with measured cloud droplet concentrations, e.g. Miles (2000).

Threshold criterion for calculations with either SACURA or LUT was the reflectance of channel 2 (0.85 μm), using a value, which approximately fits to the cloud optical thickness around 5. The cloud optical thickness is calculated at 550 nm for the LUT and 850 nm for SACURA, but cloud optical thickness is approximately wavelength-independent in this region. Calculations with both retrievals around +/−0.1 of the reflectance-selection criteria near the threshold showed a correlation factor of 0.73 for the optical thickness with a mean relative deviation of 11.3%, and 0.91 for the effective radius, with a mean relative deviation of 6.7%. The differences are within the uncertainty of the theoretical model used, e.g. the assumption of an unpolluted vertically and horizontally homogeneous cloud within a pixel.

3.3. Impact of uncertainties due to surface reflectance on optical parameters

Ships create long ship wakes with turbulent waves and they can also produce white caps and foam with increased reflectivity. For thin, semi-transparent clouds the increased reflectance might be misinterpreted as a modification of the cloud parameters. To analyze reflectance changes produced by the wake of the ship, simulations have

ACPD
6, 1023–1071, 2006

been carried out with libRadtran at 850 nm and 1640 nm, for channel 2 and channel 6 of the MODIS-instrument, which were used to calculate cloud parameters.

Figure 7 shows simulations of the top-of-atmosphere reflectances for different assumptions on the ocean surface below the cloud. The simulations were calculated for several cloud optical thicknesses, using a solar zenith angle of 60°, a satellite zenith angle of 10° and a relative azimuth angle of 45°, representative for the conditions of the examined satellite image. Lambertian ocean surface spectral reflectances (850 nm: 0.03, 1640 nm: 0.0) were used for retrieving the optical parameters via SACURA and LUT. The turbulence caused by the ship can result in white caps in a ship wake. Surface reflectances of 0.6 for 850 nm and 0.3 for 1650 nm are used for white caps (Kokhanovsky, 2004b). It can be seen from Fig. 7a that the change in reflectivity in the visible wavelength is significant and also in the near infrared (Fig. 7b) up to a simulated cloud optical thickness of 20. This results in large errors of cloud optical thickness (Fig. 7c) and effective radius (Fig. 7d). Simulations were also performed for a realistic ocean Bidirectional Reflection Distribution Function (BRDF) calculated using the methods of Cox and Munk (1954) and Nakajima and Tanaka (1983), provided by libRadtran. The lower wind speeds 1m/s and 5 m/s were used for winds above the ocean surface (see reanalysis data) and the faster wind speed of 20 m/s was used to simulate a high turbulence according to waves generated in the ship wake. The slow wind speeds produce only a slight error in the calculation for thin clouds of optical thickness of 5 and are unimportant for thicker clouds. The change in reflectance due to turbulent waves results in a somewhat larger error of the optical parameters (2.2% for the effective radius and 9.5% for the optical thickness) for clouds with a low optical thickness, caused by the change in the reflectivity at the visible wavelength.

Overall, changes in the surface reflectance of the ocean below clouds due to wind or small turbulences generated by ships result in small errors, whereas foam generated by ships could influence the retrieved parameters and possibly also the ship track detection up to a cloud optical thickness of 20 and higher.

Figure 8 shows a profile of the measured signal of the channels used for the retrieval,

0.85 μm, 1.64 μm and 2.13 μm It indicates a higher increase of the signal and also a reduced signal-to-noise of ship tracks for 1.64 μm and 2.13 μm compared to 0.85 μm. This is vice versa to the change in surface-reflectance by whitecaps, BRDF or sun glint.

Cloud modifications can be better distinguished from surface reflectance changes by adding the information of a wavelength in the near infrared. 2.13 μm were selected for the detection because it showed the best signal-to-noise ratio. We conclude also that ship tracks in otherwise clear sky conditions, identified in visible wavelength measurements (see Fig. 9), have to be classified with care, if examined without a wavelength in the near infrared.

To surely exclude these possible although unlikely problems with optically thin clouds in our analysis, a smaller scene has been selected, called “smaller selected scene”, (see Fig. 10), in addition to the entire scene, where the cloud optical thickness of the non-ship-track environmental clouds near the ship tracks are all larger than 20. The optical thickness in this subset is 20 to 30 in the no-ship-track-clouds, but increases to 45 and higher in the ship tracks. Therefore, effects of foam or turbulence are negligible in for the selected area.

3.4. Estimating the impact on the radiation field

The derived optical parameters were used to estimate changes in solar radiation for the areas below and above the cloud as well as the thermal outgoing radiation by radiative transfer calculations. Optical thickness and the effective radius have been applied to create look-up-tables for the solar flux via the radiative transfer code libRadtran (Mayer and Kylling, 2005), by using the built in k-distribution by Kato et al. (1999) to calculate integrated solar irradiance with the solver disort2 (Stamnes et al., 1988). The down-welling irradiance at the surface and the up-welling flux at top of the atmosphere were calculated for the mid-latitude winter atmosphere (AFGL-TR-86-0110, Anderson et al., 1986). Using these look-up-tables the solar flux was calculated for every pixel taking into account the local solar zenith angle of each pixel. The cloud top height was chosen to be 1000 m and the cloud-bottom height was 500 m. The mean values

ACPD
6, 1023–1071, 2006

for all low-cloud-pixels, ship-track-pixels and no-track-pixels were determined (results see Sect. 4.3), to give an estimate on the impact of ship tracks influence on both, the received solar radiation at the surface and the backscattered radiation at the top of the atmosphere.

The changes in thermal radiation of the cloud due to changes in cloud properties were also calculated via look-up-tables calculated by libRadtran. The calculations were done by using the correlated-k distribution by Fu and Liou (1992) again with the solver disort2 also using the mid-latitude winter standard atmosphere. To investigate the change in thermal radiation only by change in optical parameters, it was assumed there are no changes in cloud top height for the ship tracks, again using a cloud top-height of 1000 m together with a cloud bottom-height of 500 m.

4. Results

4.1. Detected ship tracks

Figure 10 shows the resulting analysis of the particular scene derived from the ship track mask algorithm, described in Sect. 3.1. The grey and black areas mark all low-cloud-pixels, which are susceptible for modifications due to ship emissions. The black pixels are the identified ship-track-pixels. Comparing Figs. 1, 2 and 10, it can be seen that not all ship-track-pixels are found and that a small number of pixels marked as ship-track-pixels are not inside a ship track. By using the combination of channels 7 and 2 only those ship-track-pixels were taken into account, which significantly change the backscattered radiation at top of atmosphere. For the whole scene, 6.7% of the low-cloud-pixels were identified as ship-track-pixels and 93.3% as no-ship-track-pixels. For the smaller selected scene 8.6% ship-track-pixels and 81.4% no-ship-track-pixels were identified by the algorithm. If the ship-track-pixel show significant changes of microphysical and optical parameters compared to the no ship-track-pixels is investigated in the next section.

ACPD
6, 1023–1071, 2006

4.2. Microphysical and optical cloud properties

The cloud retrieval algorithm (Sect. 3.2) was used to calculate optical and microphysical parameters of low clouds. Retrieved parameters are shown in Fig. 11. It can be seen that ship emissions result in the decrease of the effective radius (Fig. 11a). The increase of the optical thickness is also significant (Fig. 11b). Changes in the liquid water path (Fig. 12c) are not obvious, but a high increase in the droplet concentration (Fig. 12d) is seen compared with the unpolluted cloud scene results.

Figure 12 shows the smaller selected area to allow a more detailed analysis of the ship track characteristics. In this area no cloud-edges are included and also the solar zenith angle variation from 60° to 66° can be assumed as almost constant. Also, the optical thickness of the no-ship-track clouds is mostly higher than 20 (see Sect. 3.3). A significant decrease of the effective radius from 12 μm down to 6 μm is visible across the ship tracks (Fig. 12a). The optical thickness of unpolluted clouds is about 20 to 30 and is increasing in the track up to 45 and higher (Fig. 12b). Also the change in the droplet number concentration from around 100 cm^{-3} up to 800 cm^{-3} is substantial (Fig. 13d), while the liquid water path is hardly affected compared to the other plots (Fig. 12c).

Table 1 summarise the mean values of the various parameters for the low-cloud-pixel, both for the entire area as well as for the selected area for ship-track-pixels and no-ship-track-pixels. The decrease in the effective radius from 13.2 to 10.1 μm for the entire area and from 11.9 to 8.9 μm for the smaller area is evident and also an increase in cloud optical thickness from 20.7 up to 34.6 for the entire area and from 23.8 up to 30.9 for the selected area is observed. The increase in droplet number concentration is apparent if ship-track- and no-ship-track-pixels are compared. A change of the liquid water path for the entire scene is seen, but not for the smaller selected area. It is also not obvious for the areas of ship-track-pixels in Fig. 11c, so the increase of the liquid water path due to ship emissions is not certain. However, it has to be taken into account that the retrieved values are derived by looking on the top of the cloud and

ACPD
6, 1023–1071, 2006

assuming a vertically homogeneous cloud, whereas the proposals of Albrecht (1989) and Han et al. (2002) indicate an influence by emissions of the lower part of the cloud.

Figure 13 shows the resulting statistical distributions of the parameters comparing no-ship-track-pixels and ship-track-pixels for all low-cloud-pixels (A, B, C, D) and for the smaller selected area (a, b, c, d). If all low-cloud-pixels are considered (Fig. 13A), a change of the maximum of the effective radius towards smaller radii can be seen, whereas the distribution is changed towards higher values for the cloud optical thickness (Fig. 13B). The droplet number distribution shows a significant shift of the maximum from 70 cm^{-3} to 160 cm^{-3}(Fig. 13D). Droplet numbers are higher than 500 cm^{-3}, in contrast to the ones outside of the tracks. Again only a small change of the liquid water path results, but is not significant (Fig. 13C). The distribution of liquid water path in the smaller selected area does not change (Fig. 13c), whereas the change of the other parameters is more significant than in the distributions of the whole area. The distribution of the cloud optical thickness inside the tracks shows values again above 50 (Fig. 13b), which do not appear in the distribution of the outside pixels. The ship-track-pixels of the selected area also show a narrower distribution for the effective radius and the cloud optical thickness confirmed by a decrease of the standard deviation.

In summary, ship emissions of aerosols and their precursors result in an increase of the droplet number concentration and a decrease in the effective radius in the cloud. A larger number of smaller droplets for a fixed liquid water content results in the observed increase in the cloud optical thickness. There is no significant indication that more water is bound inside the cloud as the change of the liquid water path is not significant inside the tracks. The results from satellite data analysis agree with previous studies, e.g. from the MAST-experiment (Öström et al., 2000; Hobbs et al., 2000), where an increase of the droplet number concentration and a decrease of the effective radius was found, with no significant increase in the liquid water path.

ACPD
6, 1023–1071, 2006

4.3. Radiative effects

4.3.1. Changes in solar flux

Figure 14 shows down-welling solar radiation at the surface below the clouds and reflected solar radiation TOA, calculated by the method described in Sect. 3.3. In this calculation the optical parameters derived as described in Sect. 3 and depicted in Fig. 11, as well as the solar zenith angle is taken into account for each pixel. As the solar zenith angle varies over the scene from approx. 50° to 80°, the simulated surface and TOA irradiance are influenced by both, the SZA and the optical parameters. Below a ship track the solar radiation is significantly reduced compared to outside the track because the reflectance of the cloud in the track is higher. The reflected solar radiation at TOA above the ship tracks is significantly enhanced. To be more quantitatively, Table 2 shows the mean values of the down-welling solar radiation at the surface and the reflected solar radiation at TOA, averaged over all pixels with ship tracks ($E_{ship-track}$), with no ship tracks ($E_{no-ship-track}$), and all low-cloud-pixels ($E_{low-clouds}$) for the whole scene and the smaller selected area. The resulting transmitted energy below the ship-track-pixels is reduced by 2.12 and 2.47 Wm^{-2}, for the smaller selected area and the entire scene respectively. Consequently, the changed optical properties of the clouds due to ship emissions seem to modify the atmospheric energy budget. The incoming solar radiation is partly absorbed by the cloud, the surface, and the atmosphere, and partly reflected back. An increase in the reflectance of the cloud results in a cooling of the atmosphere-Earth system, observable in an increase of the up-welling flux at the top of the atmosphere (TOA) for ship-track- pixels. Calculation for the scene show an enhanced reflected radiation at TOA by 0.87 Wm^{-2} for all low-cloud-pixel and 1.56 Wm^{-2} for the smaller selected area.

When absolute radiation values (ship-track-pixels vs. no-ship-track-pixels) are compared, caution is required since the incident solar radiation at TOA depends on geographic position (i.e. on solar zenith angle) and ship tracks are not uniformly distributed over the selected scene. To quantify the magnitude of the solar zenith angle impact

on the solar flux, the variation of the average incoming irradiance TOA was simulated with the radiative transfer model for all pixels, all ship-track- and all no-ship-track-pixels for both, the full scene and the smaller selected area. The difference between all low cloud pixels and the no-ship-track-pixels is about $-0.6\,W/m^2$ (all low-cloud-pixel) to $-1.6\,W/m^2$ (smaller selected area). In addition to that, the cloud reflectance, transmittance as well as atmospheric absorption also depend on solar zenith angles. In summary, the impact of the solar zenith angle variation over the scene is of similar order of magnitude as the combined effect of changes in optical properties and solar zenith angle effects.

To separate the impact of changes in cloud parameters from ship tracks on the radiation field without the uncertainties represented by the solar zenith angle variations, radiative transfer calculations were performed assuming a mean solar zenith angle of 63° (Table 3a) for all pixels. The calculated values in Table 3 now only depend on the cloud optical properties, as the influence of a varying solar zenith angle has been eliminated.

Assuming a constant solar zenith angle, the mean value of the down-welling solar radiation at the surface below the ship-track-pixels is reduced by $43.25\,Wm^{-2}$ due to the change in the cloud parameters, compared to the no-ship-track-pixels in the entire scene. This change is comparable to the calculated discrepancy of $63\,Wm^{-2}$ between maritime and continental clouds as proposed by Kiehl (1994) for a similar solar zenith angle. At TOA ship-track-pixels reflect $40.73\,Wm^{-2}$ more than the no-ship-track-pixels for the entire scene. For the selected area the reduction of the down-welling solar radiation at the surface due to ship tracks is $21.97\,Wm^{-2}$ and the increase in TOA is $23.64\,Wm^{-2}$.

The net radiative effect of the change in cloud properties due to ships for the particular scene is estimated by calculating the difference of the absolute radiation values between all low-cloud-pixels ($E_{low-cloud}$) and the no-ship-track-pixels ($E_{no-ship-track}$). According to these values, the solar radiation at the surface is reduced on average by $2.10\,Wm^{-2}$ by the ship emissions and additional $2.00\,Wm^{-2}$ are reflected back at TOA.

ACPD
6, 1023–1071, 2006

Table 4a also shows the values for the smaller selected area with an on average decrease in the radiation of 2.04 Wm^{-2} at the surface and an increase in the outgoing radiation at TOA of 2.19 Wm^{-2} due to the ship emissions.

For the same spatial distribution of cloud and ship track properties, the solar radiation has been also calculated for other solar zenith angles to get an estimate of the dependence of the radiation changes by ship tracks on the solar zenith angle (Tables 3b–d). For a smaller solar zenith angle of 50° the scene average radiation decreases to $-3.63\,Wm^{-2}$ at the surface and increases to 3.36 Wm^{-2} at TOA. For larger mean solar zenith angle of 70° the scene average change is $-1.35\,Wm^{-2}$ at the surface and 1.29 Wm^{-2} for the backscattered radiation at TOA. For an even large solar zenith angle of 80° the change is only $-0.51\,Wm^{-2}$ for the surface and only 0.49 Wm^{-2} for TOA. In summary, smaller SZA result in an amplification of the solar radiation changes on the surface and TOA, whereas for high solar zenith angles the effect will vanish. According to Durkee et al. (2000b), ship tracks have an average lifetime of 7.5 h, so the solar zenith angle dependence must be included when estimating the radiative impact of ship tracks.

4.3.2. Changes in thermal irradiance

To estimate the importance of ship tracks on the radiation budget, also changes in thermal radiation of the cloud have to be taken into account. Table 4 shows the mean values for the thermal radiation of the cloud. Compared to the value of no-ship-track-pixels the thermal radiation for the ship-track-pixels is decreased. Subtracting the mean no-ship-track-value from the mean low-cloud-value, we can calculate the thermal effect of the ship tracks. This difference amounts to 0.43 Wm^{-2} for the whole scene. The magnitude for the selected area is 0.43 Wm^{-2} as well.

ACPD
6, 1023–1071, 2006

4.3.3. Net-radiative effect at TOA

Combining solar and thermal effect gives an estimation of the net-effect of cloud parameter changes by ship tracks for the particular scene under the assumption of a constant solar zenith angle. The calculated net-effect at TOA is a cooling of the atmosphere by 1.57 Wm^{-2} for the whole scene and 1.76 Wm^{-2} for the smaller selected area.

The results show that anthropogenic emissions from ships influence maritime clouds and affect the radiative energy budget at the surface and also the reflected radiation at TOA. Ship tracks enhance solar reflection, resulting in a cooling of the atmosphere, while in the thermal infrared they tend to reduce the outgoing longwave radiation (warming). For the scene investigated in this work, the net-effect is a cooling of 1 to 2 W/m^2 depending on how the solar zenith angle impact is estimated.

Not included in this analysis are the diurnal cycle of maritime stratiform clouds (Cahalan et al., 1994; Norris, 1998b), the influence of ship emissions on the cloud properties at night time as well as the lifetime of ship tracks, and the behaviour during night-time.

4.4. Potential drizzle suppression

Even though we do not find a significant change in the liquid water path indicating drizzle suppression as proposed by Albrecht et al. (1989) one may also study a hypothetical influence of ship emissions on the latent heat. The effective radius could be used to estimate drizzle suppression areas. Rosenfeld and Gutman (1994) and Masunaga at al. (2002) found precipitation if the effective radius of cloud droplets at cloud top was higher than 14 μm. There are small areas in the analyzed scene, where the effective radius is higher than 14 μm outside and smaller than 14 μm inside the ship tracks. These areas may therefore serve as a proxy for drizzle suppression. Figure 15 shows the areas, where drizzle suppression could occur. These areas of possible drizzle suppression inside the ship tracks extend over several square kilometres and could significantly affect the latent heat budget of the area. This effect may not be neglected when looking at global impacts of ship emissions on the atmospheric energy budget.

ACPD
6, 1023–1071, 2006

5. Summary and conclusion

An algorithm has been developed to determine ship tracks from satellite data in an automated way. A scene on 10 February 2003 was chosen to extract the optical and microphysical cloud modifications from ship emissions using Terra-MODIS satellite data. A combination of the semi-analytical approach SACURA with a look-up-table for optically thin clouds was used to calculate cloud properties.

It was demonstrated that the wake of a ship may influence the ship track detection and the optical parameters due to changes of the surface reflectance and that ship tracks in otherwise clear sky conditions have to be examined with care. Adding a channel in the near infrared helps to exclude errors by whitecaps, BRDF and sun glint.

It has also been shown that ship emissions modify existing clouds by decreasing the effective radius, while they increase droplet concentration and optical thickness. On average, the optical thickness was increased from 20.7 up to 34.6 and the effective radius was decreased from 13.2 μm to 10.1 μm. The calculated average droplet number concentration increased from 79 up to 210 cm^{-3}. There was no significant evidence for a change in liquid water path. The results basically agree with the theory and with the MAST experiment (Öström et al., 2000; Hobbs et al., 2000): Low clouds of the maritime boundary layer have less cloud condensation nuclei than clouds over land; in consequence, their droplet radius is larger. Injection of aerosols and their pre-cursors by ships results in more CCNs causing the mean droplet radius to decrease and the droplet number concentration to increase.

The derived parameters were used to calculate changes in the radiative energy budget below and above the cloud. The mean values show a decrease of 43.25 Wm^{-2} for the surface radiation below ship tracks and an increase of 40.73 Wm^{-2} for the increased reflectivity at TOA. If the whole low-cloud area with 6.7% ship-track-pixels is taken into account, a decrease in the radiation at the surface of 2.10 Wm^{-2} and an increase of 2.00 Wm^{-2} in backscattered solar radiation was found, when assuming a constant solar zenith angle for the scene. Also a reduced thermal radiation of

ACPD
6, 1023–1071, 2006

$0.43\,\mathrm{Wm}^{-2}$ was found reducing the net-radiative effect on TOA. The resulting radiative forcing due to ship tracks for the satellite scene was estimated to be a cooling of $-1.57\,\mathrm{Wm}^{-2}$ of the atmosphere-Earth system. The influence of the thermal radiation is not negligible and the temporal behaviour of ship tracks have to be further investigated.

Assuming that drizzle can be estimated with the help of the effective radius, drizzle suppression over a substantial area is possible. This indicates that not only the radiative budget is affected by ship emissions, but also the budget of latent heat.

The results showed that modifications of clouds by international shipping can be an important contributor to climate and precipitation pattern change. The problem has to be studied further to allow to systematically assess the global impact.

Acknowledgements. We wish to thank the MODIS NASA team for providing the MODIS data products in such a straightforward way on their website.

Special thanks go to A. Lauer, T. Zinner and U. Schumann (DLR) for helpful discussions.

This work has been supported by the Junior Research Group SeaKLIM, which is funded by the German Helmholtz-Gemeinschaft, and the Deutsches Zentrum für Luft- und Raumfahrt e.V. (DLR). We also acknowledge support of the DFG project BU 688/8-1.

References

Ackermann, A. S., Toon, O. B., Taylor, J. P., Johnson, D. W., Hobbs, P. V., and Ferek, R. J.: Effects of Aerosols on Cloud Albedo: Evaluation of Twomey's Parameterisation of Cloud Susceptibility Using Measurements of Ship Tracks, J. Atmos. Sci., 57, 2684–2695, 2000.

Albrecht, B. A.: Aerosols, cloud microphysics, and fractional cloudiness, Science, 245, 1227–1230, 1989.

Anderson, G. P., Clough, S. A., Kneizys, F. X., Chetwynd, J. H., and Shettle, E. P.: AFGL Atmospheric Constituent Profiles (0–120 km) , AFGL-TR-86-0110, AFGL (OPI), Hanscom AFB, MA 01736, 1986.

Beirle, S., Platt, U., von Glasow, R., Wenig, M., and Wagner, T.: Estimate of nitrogen oxide emissions from shipping by satellite remote sensing, Geophys. Res. Lett., 31, L18102, doi:10.1029/2004GL020312, 2004.

Christopher, S. A. and Zhan, J.: Shortwave Aerosol Radiative Forcing from MODIS and CERES observations over the oceans, Geophys. Res. Lett., 29, 1859–1865, 2002.
Cahalan, R. F., Ridgway, W., Wiscombe, W. J., Bell, T. J., and Snider, J. B.: The albedo of fractal stratocumulus clouds, J. Atmos. Sci., 51, 2434–2455, 1994.
Capaldo, K., Corbett, J. J., Kasibhatla, P., Fischbeck, P. S., and Pandis, S. N.: Effects of ship emissions on sulphur cycling and radiative climate forcing over the ocean, Nature, 400, 743–746, 1999.
Coakley Jr., J. A., Durkee, P. A., Nielsen, K., Taylor, J. P., Platnick, S., Albrecht, B. A., Babb, D., Chang, F. L., Tahnk, W. R., Bretherton, C. S., and Hobbs, P. V.: The Appearance and Disappearance of Ship Tracks an Large Spatial Scales, J. Atmos. Sci., 57 , 2765–2778, 2000.
Conover, J. H.: Anomalous Cloud Lines, J. Atmos. Sci., 23, 778–785, 1966.
Cox, C. and Munk, W.: Statistics of the sea surface derived from sun glitter, J. Marine Res., 13, 198–227, 1954.
Davis, D. D., Grodzinsky, G., Kasibhatla, P., Crawford, J., Chen, G., Liu, S., Bandy, A., Thornton, D., Guan, H., and Sandholm, S.: Impact of Ship Emissions on Marine Boundary Layer NO_x and SO_2 Distributions over the Pacific Basin, Geophys. Res. Lett., 28, 235–238, 2001.
Deirmendjian, A.: Electromagnetic Scattering on Spherical Polydispersions, Elsevier, Amsterdam, 1969.
Durkee, P. A., Noone, K. J., and Bluth, R. T.: The Monterey Ship Track Experiment, J. Atmos. Sci., 57, 2523–2541, 2000a.
Durkee, P. A., Chartier, R. E., Brown, A., Trehubenko, E. J., Rogerson, S. D., Skupniewicz, C., Nielsen, K. E., Platnick, S., and King, M. D.: Composite Ship Track Characteristics, J. Atmos. Sci., 57, 2542–2553, 2000b.
Durkee, P. A., Noone, K. J., Ferek, R. J., Johnson, D. W., Taylor, J. P., Garrett, T. J., Hobbs, P. V., Hudson, J. G., Bretherton, C. S., Innis, G., Frick, G. M., Hoppel, W. A., O'Dowd, C. D., Russel, L. M., Gasparovic, R., Nielsen, K. E., Tessmer, S. A., Öström, E., Osbourne, S. R., Flagan, R. C., Seinfeld, J. H., and Rand, H.: The Impact of Ship-Produced Aerosols on the Microstructure and Albedo of Warm Marine Stratocumulus Clouds: A Test of MAST Hypothesis 1i and 1ii, J. Atmos. Sci., 57, 2554–2569, 2000c.
Endresen, O., Sorgard, E., Sundet, J. K., Dalsoren, S. B., Isaksen, I. S. A., Berglen, T. F., and Gravir, G.: Emission from international sea transportation and environmental impact, J. Geophys. Res., 108, 4560, doi:10.1029/2002JD00JD002898, 2003.

Entec UK Limited: European Commission: Quantification of emissions from ships associated with ship movements between ports in the European Community, Final Report, July 2002, Entec UK Limited, 2002.
EPA: United States Environmental Protection Agency Air and Radiation, Analysis of Commercial Marine Vessels Emissions and Fuel , EPA420-R-00-002, February 2000.
Eyring, V., Köhler, H. W., van Aardenne, J., and Lauer, A.: Emissions from international shipping: 1. The last 50 years, J. Geophys. Res., 110, D17305, doi:10.1029/2004JD005619, 2005a.
Eyring, V., Köhler, H. W., Lauer, A., and Lemper, B.: Emissions from international shipping: 2. Impact of future technologies on scenarios until 2050, J. Geophys. Res., 110, D17306, doi:10.1029/2004JD005620, 2005b.
Facchini, M. C., Mircea, M., Fuzzi, S., and Charlson, R. J.: Cloud albedo enhancement by surface-active organic solutes in growing droplets, Nature, 401, 257–259, 1999.
Ferek, R. J., Garrett, T., Hobbs, P. V., Strader, S., Johnson, D., Taylor, J. P., Nielsen, K., Ackermann, A. S., Kogan, Y., Liu, Q., Albrecht, B. A., and Babb, D.: Drizzle Suppression in Ship Tracks, J. Atmos. Sci., 57, 2707–2728, 2000.
Frick, G. M. and Hoppel, W. A.: Airship Measurements of Ship's Exhaust Plumes and Their Effect on Marine Boundary Layer Clouds, J. Atmos. Sci., 57, 2625–2648, 2000.
Fu, Q. and Liou, K. N.: On the correlated k-distribution method for radiative transfer in nonhomogeneous atmospheres, J. Atmos. Sci., 49, 2139–2156, 1992.
Han, Q., Rossow, W. B., Chou, J., and Welch, R. M.: Global variation of column droplet concentration in low-level clouds, Geophys. Res. Lett., 25(9), 1419–1422, 1998.
Han, Q., Rossow, W. B., Zeng, J., and Welch, R.: Three different behaviors of liquid water path of water clouds in aerosol-cloud interactions, J. Atmos. Sci., 59, 726–735, 2002 .
Hobbs, P. V., Garrett, T. J., Ferek, R. J., Strader, S. R., Hegg, D. A., Frick, G. M., Hoppel, W. A., Gasparovic, R. F., Russell, L. M., Johnson, D. W., O'Dowd, C., Durkee, P. A., Nielsen, K. E., and Innis, G.: Emissions from Ships with their respect to clouds, J. Atmos. Sci., 57, 2570–2590, 2000.
Hooper, W. P. and James, E. J.: Lidar Observations of Ship Plumes, J. Atmos. Sci., 57, 2649–2566, 2000.
Hudson, J. G., Garrett, T. J., Hobbs, P. V., Strader, S. R., Xie, Y., and Yum, S. S.: Cloud Condensation Nuclei and Ship Tracks, J. Atmos. Sci., 57, 2696–2707, 2000.
Johnson, W. D., Osborne, S., Wood, R., Suhre, K., Quinn, P. K., Bates, T., Andreae, M. O.,

Noone, K. J., Glantz, P., Bandy, B., Rudolph, J., and O'Dowd, C.: Observations of the evolution of the aerosol, cloud and boundary-layer characteristics during the 1st ACE-2 Lagrangian experiment, Tellus, 52B, 348–374, 2000.
Kasibhatla, P., Levy II, H., Moxim, W. J., Pandis, S. N., Corbett, J. J., Peterson, M. C., Honrath, R. E., Frost, G. J., Knapp, K., Parrish, D. D., and Ryerson, T. B.: Do emissions form ships have a significant impact on concentration of nitrogen oxides in the marine boundary layer?, Geophys. Res. Lett., 27(15), 2229–2233, 2000.
Kato, S., Ackermann, T. P., Mather, J. H., and Clothiaux, E. E.: The k-distribution method and correlated-k approximation for a shortwave radiative transfer model, J. Quant. Spectrosc. Radiat. Trans., 62, 109–121, 1999.
Kiehl, J. T.: Sensitivity of GCM climate simulation to differences in continental versus maritime cloud droplet size, J. Geophys. Res., 99, 23 107–23 115, 1994.
King, M. D., Herring, D. D., and Diner, D. J.: The Earth Observing System (EOS): A space based program for asessing mankind's impact on the global environment, Opt. Photon News, 6, 34–39, 1995.
Kokhanovsky, A. A., Rozanov, V. V., Zege, E. P., Bovensmann, H., and Burrows, J. P.: A semi-analytical cloud retrieval algorithm using backscattered radiation in 0.4–2.4 micrometers spectral range, J. Geophys. Res., 108(D1), 4008, doi:10.1029/2001JD001543, 2003.
Kokhanovsky, A.: Optical properties of terrestrial clouds, Earth Sci. Rev., 64, 189–241, 2004a.
Kokhanovsky, A.: Spectral reflectance of whitecaps, J. Geophys. Res., 109, C05021, doi:10.1029/2003JC002177, 2004b.
Lawrence, M. G. and Crutzen, P. J.: Influence of NO_x emissions from ships on tropospheric photochemistry and climate, Nature, 402, 167–170, 1999.
Lensky, I. M. and Rosenfeld, D.: Satellite-Based Insights into Preciptitation Formation Processes in Continental and Maritime Convective Clouds at Nighttime, J. Appl. Meteorol., 42, 1227–1233, 2003.
Liu, Q., Kogan, Y. L., Lilly, D. K., Johnson, D. W., Innis, G. E., Durkee, P. A., and Nielsen, K. E.: Modelling of Effluent Transport and Its Sensitivity to Boundary Layer Structure, J. Atmos. Sci., 57, 2779–2791, 2000.
Lohmann, U.: Possible Aerosol Effects on Ice Clouds via Contact Nucleation, J. Atmos. Sci., 59, 647–656, 2002.
Masunaga, H., Nakajima, T. Y., Nakajima, T., Kachi, M., and Suzuki, K.: Physical properties of maritime low clouds as retrieved by combined use of Tropical Rainfall Measuring Mission

(TRMM) Microwave Imager and Visible/Infrared Scanner 2. Climatology of warm clouds and rain, J. Geophys. Res., 107, 4367, doi:10.1029/2001JD1269, 2002.

Mayer, B., Seckmeyer, G., and Kylling, A.: Systematic longterm comparison of spectral UV measurements and UVSPEC modeling results (libRadtran-Homepage: http://www.libRadtran.org), J. Geophys. Res., 102(D7), 8755–8768, 1997.

Mayer, B. and Kylling, A.: Technical note: The libRadtran software package for radiative transfer calculations, description and examples of use, Atmos. Chem. Phys., 5, 1855–1877, 2005, SRef-ID: 1680-7324/acp/2005-5-1855.

McInnes, L. M., Quinn, P. K., Covert, D. S., and Anderson, T. L.: Gravimetric Analysis, Ionic Composition and Associated Water Mass of the Marine Aerosol, Atmos. Environ., 30, 869–884, 1996.

Miles, N. L., Verlinde, J., and Clothiaux, E. E.: Cloud Droplet Size Distributions in Low-Level Stratiform Clouds, J. Atmos. Sci., 57, 295–311, 2000.

Nakajima, T. and Tanaka, M.: Effect of wind-generated waves on the transfer of solar radiation in the atmosphere-ocean system, J. Quant. Spectrosc. Radiat. Trans., 29, 521–537, 1983.

Nauss, T., Kokhanovsky, A. A., Nakajima, T. Y., Reudenbach, C., and Bendix, J.: The intercomparison of selected cloud retrieval algorithms, Atmos. Res., 78, 46–78, 2005.

Noone, K. J., Öström, E., Ferek, R. J., Garrett, T., Hobbs, P. V., Johnson, D. W., Taylor, J. P., Russell, L. M., Fragan, R. C., Seinfeld, J. H., O'Dowd, C. D., Smith, M. H., Durkee, P. A., Nielsen, K., Hudson, J. G., Pockalny, R. A., de Bock, L., van Grieken, R. E., Gasparovic, R. F., and Brooks, I.: A Case Study of Ships Forming and Not Forming Tracks in Moderately Polluted Clouds, J. Atmos. Sci., 57, 2729–2747, 2000a.

Noone, K. J., Johnson, D. W., Taylor, J. P., Ferek, R. J., Garrett, T., Hobbs, P. V., Durkee, P. A., Nielsen, K., Öström, E., O'Dowd, C., de Bock, L., van Grieken, R. E., Hudson, J. G., Brooks, I., Gasparovic, R. F., and Pockalny, R. A.: A Case Study of Ship Track Formation in Polluted Marine Boundary Layer, J. Atmos. Sci., 57, 2748–2764, 2000b.

Norris, J. R.: Low Cloud Type over the Ocean from Surface Observations. Part I: Relationship to Surface Meteorology and the Vertical Distribution of Temperature and Moisture, J. Climate, 11(3), 369–382, 1998a.

Norris, J. R.: Low Cloud Type over the Ocean from Surface Observations. Part II: Geographical and Seasonal Variations, J. Climate, 11(3), 383–403, 1998b.

O'Dowd, C. D., Smith, M. H., Consterdine, I. E., and Lowe, J. A.: Marine Aerosol, Sea-Salt and the marine Sulphur Cycle: A Short Review, Atmos. Environ., 31, 73–80, 1997.

O'Dowd, C. D., Facchini, M. C., Cavalli, F., Ceburnis, D., Mircea, M., Decesari, S., Fuzzi, S., Yoon, Y. J., and Putaud, J. P.: Biogenically-driven organic contribution to marine aerosol, Nature, 431, 676–680, doi:10.1038/nature02959, 2004.

Öström, E., Noone, K. J., and Pockalny, R. A.: Cloud Droplet Residual Particle Microphysics in Marine Stratocumulus Clouds Observed during the Monterey Area Ship Track Experiment, J. Atmos. Sci., 57, 2671–2683, 2000.

Platnick, S., Durkee, P. A., Nielsen, K., Taylor, J. P., Tsay, S. C., King, M. D., Ferek, R. J., Hobbs, P. V., and Rottman, J. W.: The Role of Background Cloud Microphysics in the Radiative Formation of Ship Tracks, J. Atmos. Sci., 57, 2607–2624. 2000.

Porch, W. M., Kao, C. Y., Buckwald, M. I., Unruh, W. P., Durkee, P. A., Hindman, E. E., and Hudson, J. G.: The effects of external forcing on the marine boundary layer: Ship trails and a solar eclipse, Global Atmos. Ocean System, 3, 323–340, 1995.

Radke, L. F., Coakley Jr., J. A., and King, M. D.: Direct and Remote Sensing Observations of the Effects of Ships on Clouds, Science, 346, 1146–1149, 1989.

Richter, A., Eyring, V., Burrows, J. P., Bovensmann, H., Lauer, A., Sierk, B., and Crutzen, P. J.: Satellite Measurements of NO2 from Internal Shipping Emissions, Geophys. Res. Lett., 31, L23110, doi:10.1029/2004GL020822, 2004.

Rosenfeld, D. and Gutman, G.: Retrieving microphysical properties near the tops of potential rain clouds by multispectral analysis of AVHRR data, Atmos. Res., 34, 259–283, 1994.

Russel, L. M., Noone, K. J., Ferek, R. J., Pockalny, R. A., Flagan, R. C., and Seinfeld, J. H.: Combustion Organic Aerosol as Cloud Condensation Nuclei in Ship Tracks, J. Atmos. Sci., 57, 2591–2606, 2000.

Seinfeld, J. H. and Pandis, S. N.: Atmospheric Chemistry and Physics, John Wiley and Sons, Inc., 1997.

Simmons, A. J. and Gibson, J. K. (Eds.): ERA-40 Project plan. ERA-20 Project Rep. 1, ECMWF, 62 p., 2000.

Stamnes, K., Tsay, S. C., Wiscombe, W., and Jayaweera, K.: Numerically stable algorithmfor discrete-ordinate-method radiative transfer in multiple scatteringand emitting layered media, Appl. Opt., 27, 2502–2509, 1988.

Taylor, J. P., Glew, M. D., Coakley Jr., J. A., Tahnk, W. R., Platnick, S., Hobbs, P. V., and Ferek, R. J.: Effects of Aerosols on the Radiative Properties of Clouds, J. Atmos. Sci., 57, 2656–2670, 2000.

Twomey, S., Howell, H. B., and Wojciechowski, T. A.: Comments on Anomalous cloud lines, J.

Atmos. Sci., 25, 333–334, 1968.
Twomey, S.: Pollution and the planetary albedo, Atmosph. Environ., 8, 1251–1256, 1974.
Wang, J., Rossow, W. B., and Zhang, Y.: Cloud vertical structure and its variation from a 20-yr global rawinsonde dataset, J. Climate, 13, 3041–3056, 2000.
World Bunkering: Issue 9, Number 3, August, 2004.

Table 1. Mean values of cloud parameters and standard deviation (STD) in parenthesis.

	low-cloud-pixels	no-ship-track-pixels	ship-track-pixels
All low-cloud-pixel			
effective radius (μm)	13.0 (4.0)	13.2 (4.0)	10.1 (2.5)
optical thickness	21.4 (11.1)	20.7 (10.4)	34.6 (14.5)
liquid water path (gm^{-2})	174 (122)	172 (122)	227 (120)
droplet number (cm^{-3})	85 (61.7)	79 (82.8)	210 (112.6)
Smaller selected scene			
effective radius (μm)	11.6 (3.9)	11.9 (3.8)	8.9 (2.3)
optical thickness	24.4 (10.5)	23.8 (10.2)	30.9 (11.8)
liquid water path (gm^{-2})	180 (102)	180 (96)	176 (102)
droplet number (cm^{-3})	115 (60)	101 (46)	255 (101)

ACPD
6, 1023–1071, 2006

Table 2. Mean values of the transmitted solar flux at the surface and reflected radiation at the top of atmosphere, STD in parenthesis.

	low-cloud-pixels $E_{low-cloud}$	no-ship-track-pixels $E_{no-ship-track}$	ship-track-pixels $E_{ship-track}$	Difference $E_{low-cloud}$–$E_{no-ship-track}$
All low-cloud-pixel				
Surface (Wm^{-2})	127.62 (61.06)	130.09 (61.02)	78.69 (36.13)	−2.47
TOA (Wm^{-2})	336.24 (55.94)	335.37 (56.89)	353.52 (26.18)	0.87
Smaller Selected scene				
Surface (Wm^{-2})	113.35 (28.27)	115.47 (27.47)	92.65 (27.57)	−2.12
TOA (Wm^{-2})	349.78 (16.19)	348.22 (15.63)	365.08 (13.31)	1.56

ACPD
6, 1023–1071, 2006

Table 3a. Mean values of solar radiation at the surface and TOA for a fixed solar zenith angle of 63°, standard deviation in parenthesis.

fixed sza=63°	low-cloud-pixels $E_{low-cloud}$	no-ship-track-pixels $E_{no-ship-track}$	ship-track-pixels $E_{ship-track}$	Difference $E_{low-cloud}$–$E_{no-ship-track}$
All low-cloud-pixel				
Surface (Wm^{-2})	124.20 (44.99)	126.30 (44.75)	83.05 (28.88)	−2.10
TOA (Wm^{-2})	332.12 (38.17)	330.12 (37.79)	370.85 (23.51)	2.00
Smaller selected scene				
Surface (Wm^{-2})	113.49 (44.10)	115.53 (44.19)	93.56 (27.87)	−2.04
TOA (Wm^{-2})	343.48 (37.44)	341.29 (37.32)	364.93 (22.76)	2.19

ACPD
6, 1023–1071, 2006

Table 3b. Same as Table 3a, but for a solar zenith angle of 50°.

fixed sza=50°	low-cloud-pixels $E_{low-cloud}$	no-ship-track-pixels $E_{no-ship-track}$	ship-track-pixels $E_{ship-track}$	Difference $E_{low-cloud}-E_{no-ship-track}$
All low-cloud-pixel				
Surface (Wm^{-2})	213.90 (77.71)	217.53 (77.28)	142.74 (49.83)	−3.63
TOA (Wm^{-2})	442.37 (65.22)	439.01 (64.60)	508.08 (40.01)	3.36
Smaller selected scene				
Surface (Wm^{-2})	195.33 (76.17)	198.86 (76.30)	160.85 (48.06)	−3.53
TOA (Wm^{-2})	461.39 (63.96)	457.70 (63.79)	497.47 (39.11)	3.69

ACPD
6, 1023–1071, 2006

Table 3c. Same as Table 3a, but for a solar zenith angle of 70°.

fixed sza=70°	low-cloud-pixels $E_{low-cloud}$	no-ship-track-pixels $E_{no-ship-track}$	ship-track-pixels $E_{ship-track}$	Difference $E_{low-cloud}$–$E_{no-ship-track}$
All low-cloud-pixel				
Surface (Wm^{-2})	80.69 (29.11)	82.04 (28.94)	54.02 (18.74)	−1.35
TOA (Wm^{-2})	258.62 (24.84)	257.33 (24.58)	284.02 (18.08)	1.29
Smaller selected scene				
Surface (Wm^{-2})	73.76 (28.53)	75.08 (28.59)	60.86 (18.08)	−1.32
TOA (Wm^{-2})	266.14 (24.36)	264.70 (24.28)	280.27 (14.81)	1.44

ACPD
6, 1023–1071, 2006

Table 3d. Same as Table 3a, but for a solar zenith angle of 80°.

fixed sza=80°	low-cloud-pixels $E_{low-cloud}$	no-ship-track-pixels $E_{no-ship-track}$	ship-track-pixels $E_{ship-track}$	Difference $E_{low-cloud}-E_{no-ship-track}$
All low-cloud-pixel				
Surface (Wm^{-2})	30.44 (10.89)	30.95 (10.83)	20.44 (7.05)	−0.51
TOA (Wm^{-2})	134.59 (9.37)	134.10 (9.27)	144.26 (5.77)	0.49
Smaller selected scene				
Surface (Wm^{-2})	27.86 (10.67)	28.36 (10.69)	23.02 (6.80)	−0.50
TOA (Wm^{-2})	137.47 (9.19)	136.91 (9.16)	142.88 (5.59)	0.56

ACPD
6, 1023–1071, 2006

Table 4. Mean values of outgoing longwave radiation at top of atmosphere.

	low-cloud-pixels $E_{low-cloud}$	no-ship-track-pixels $E_{no-ship-track}$	ship-track-pixels $E_{ship-track}$	Difference $E_{low-cloud}$–$E_{no-ship-track}$
All low-cloud-pixel Emission (Wm^{-2})	182.91 (9.01)	183.34 (8.94)	174.45 (5.86)	−0.43
Smaller selected scene Emission (Wm^{-2})	180.71 (4.86)	181.14 (4.67)	176.51 (4.74)	−0.43

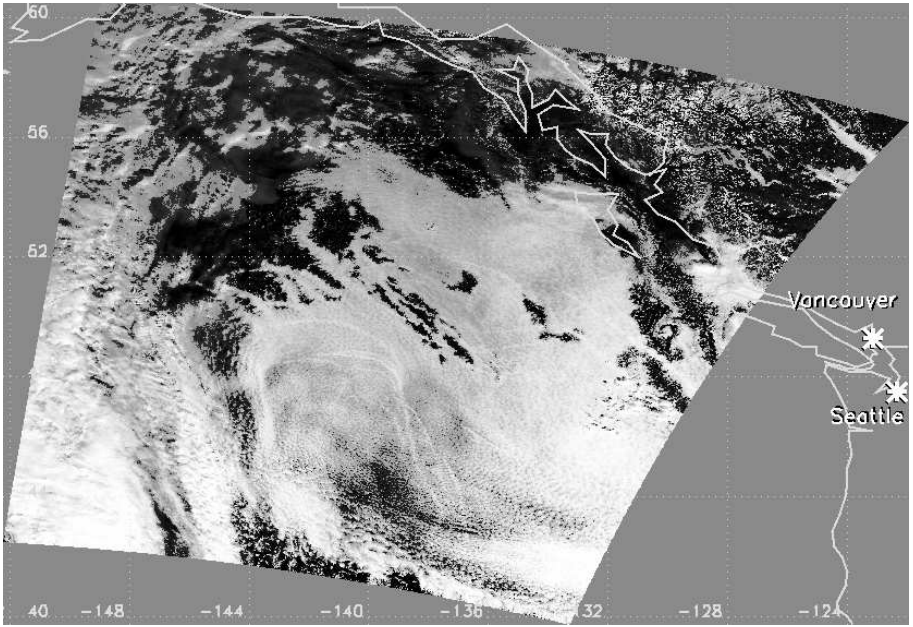

Fig. 1. Reflectance in channel 2 (0.85 μm), Terra-MODIS, 10 February 2003, from 153° to 120° west and 40° to 60° north.

ACPD

6, 1023–1071, 2006

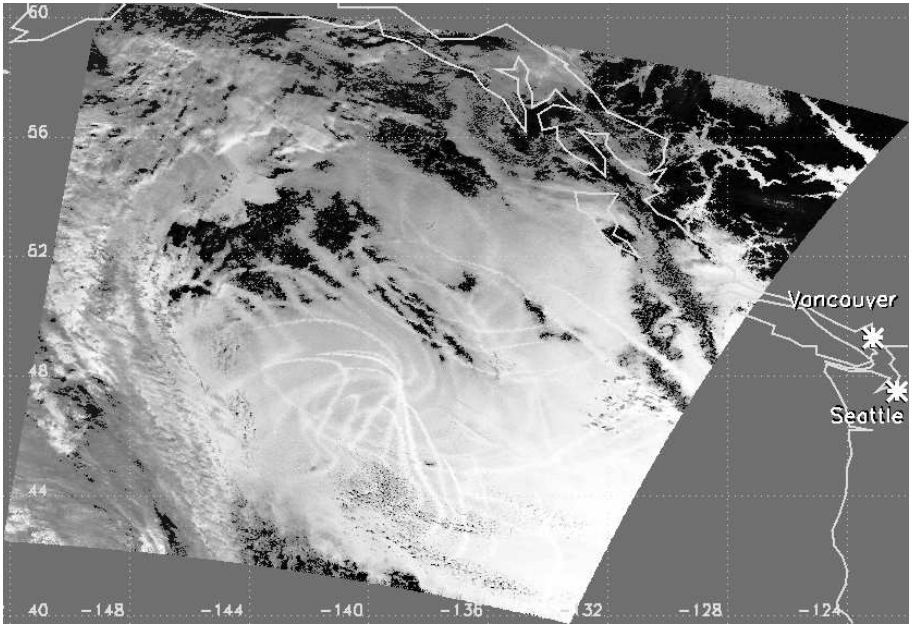

Fig. 2. Same as Fig. 1, but for 2.13 μm-channel.

ACPD
6, 1023–1071, 2006

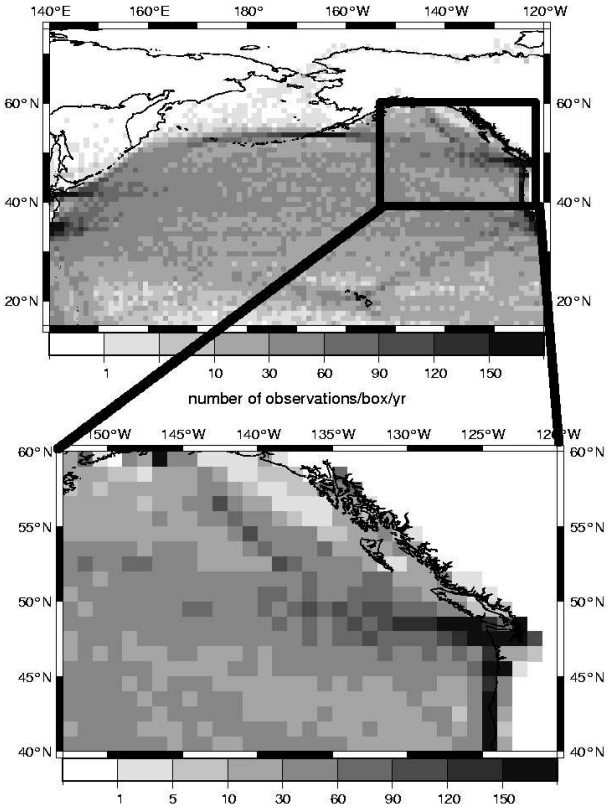

Fig. 3. Vessel traffic density of the total fleet for the year 2000 between 140° E to 120° W and 15° N to 75° N. Data are taken from Endresen et al. (2003).

ACPD

6, 1023–1071, 2006

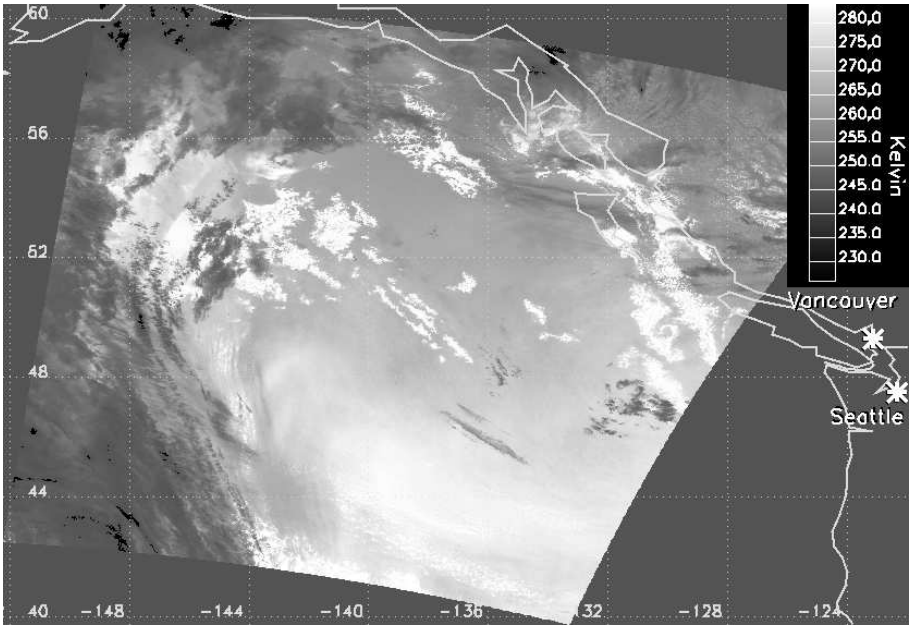

Fig. 4. Temperature of the selected scene in Kelvin, derived from satellite data (11 μm).

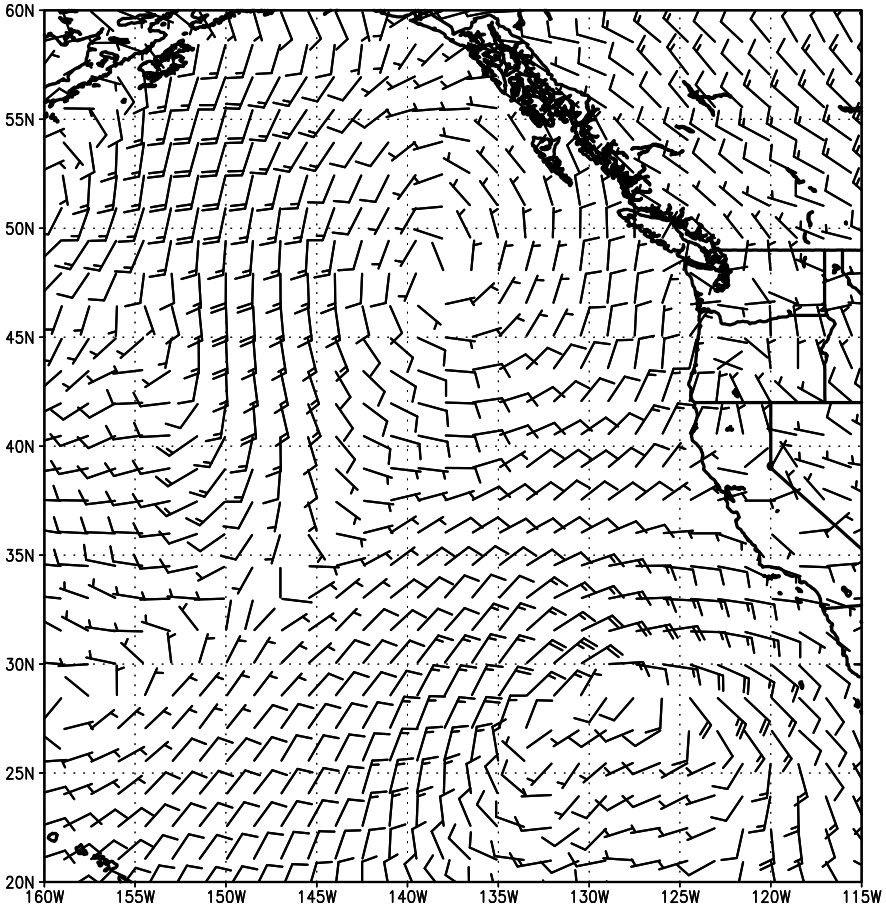

Fig. 5. Wind field from ECMWF reanalysis data on 10 February 2003 at 18:00 UTC.

ACPD

6, 1023–1071, 2006

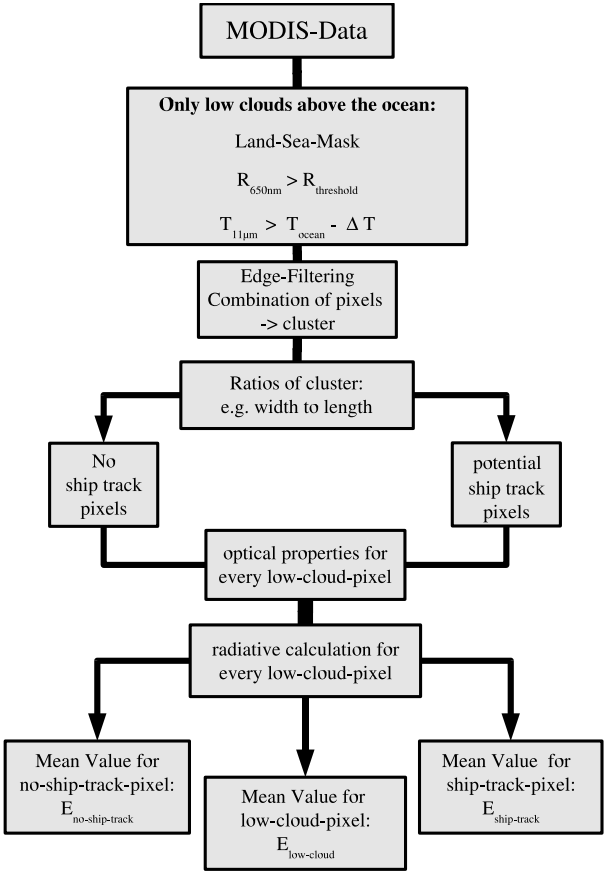

Fig. 6. Flow chart of the ship-track-algorithm that has been used in this study to calculate microphysical and optical properties of ship tracks and their radiative effect.

ACPD
6, 1023–1071, 2006

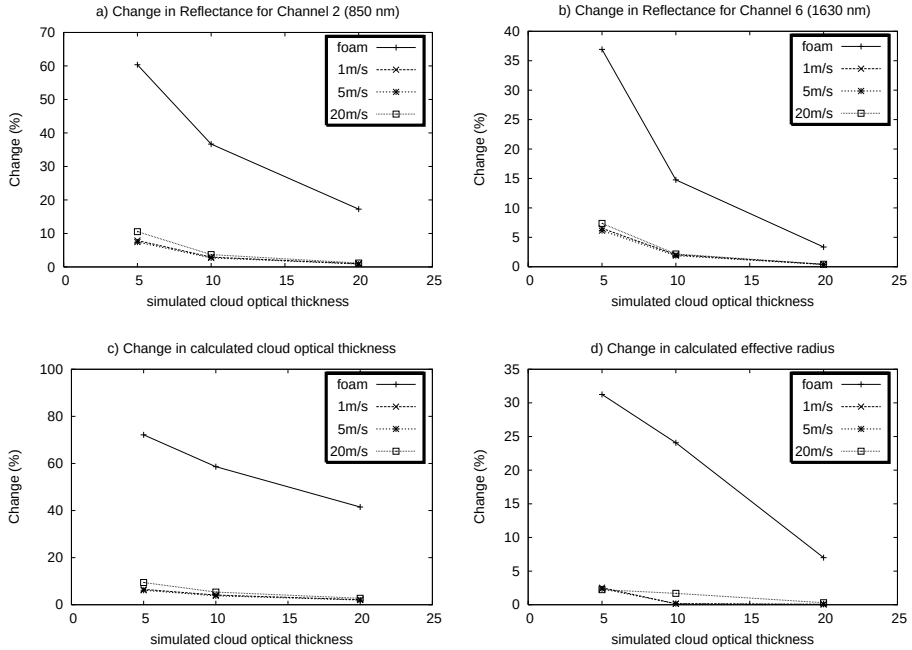

Fig. 7. Changes in simulated reflectivity (TOA) due to changes in surface reflection by foam or turbulences for channel 2 **(a)** and for channel 6 **(b)** and resulting errors in calculation of optical thickness **(c)** and effective radius **(d)**.

ACPD
6, 1023–1071, 2006

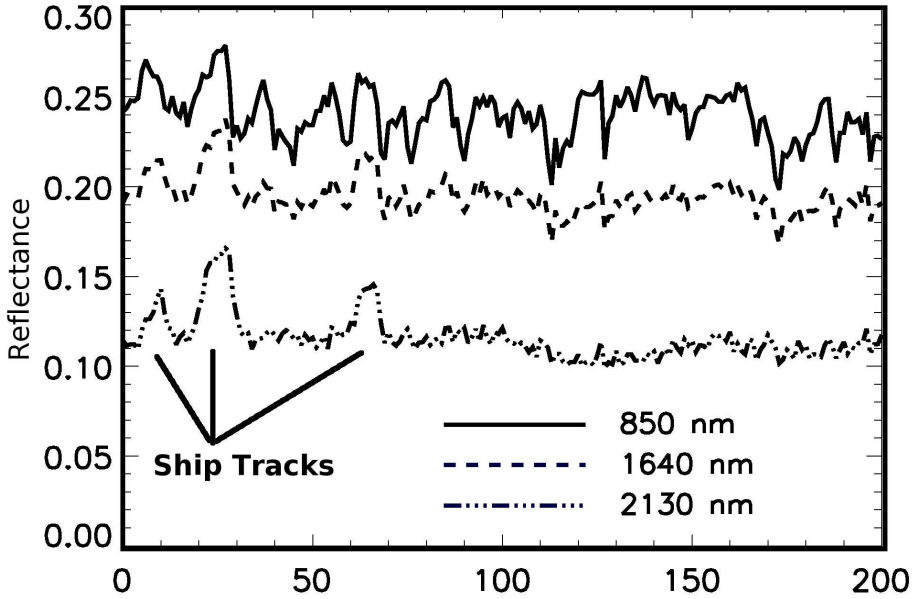

Fig. 8. Cross-section of measured reflectances with ship tracks taken from selected satellite scene (compare Fig. 10, y-coordinates: 600–800, x-coordinate: 700).

ACPD
6, 1023–1071, 2006

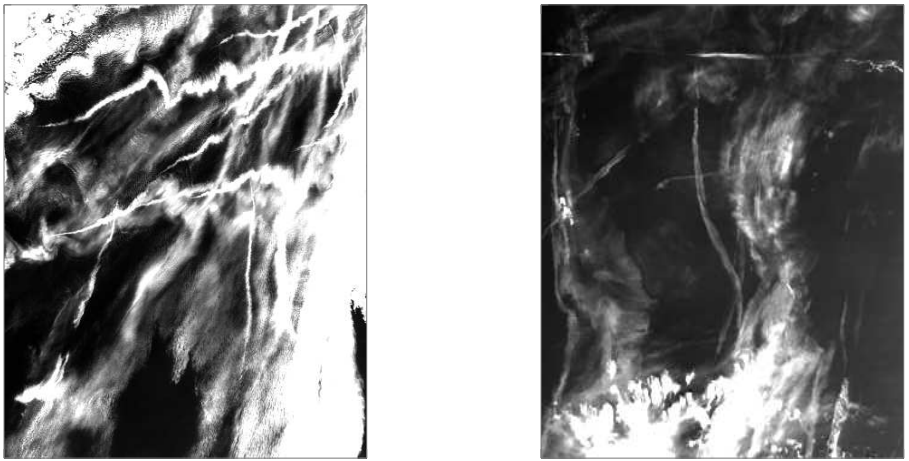

Fig. 9. Possible ship tracks, Terra-MODIS, 27 January 2003 and 30 June 2002 and, Golf of Biscay (France), channel 1 (620 nm).

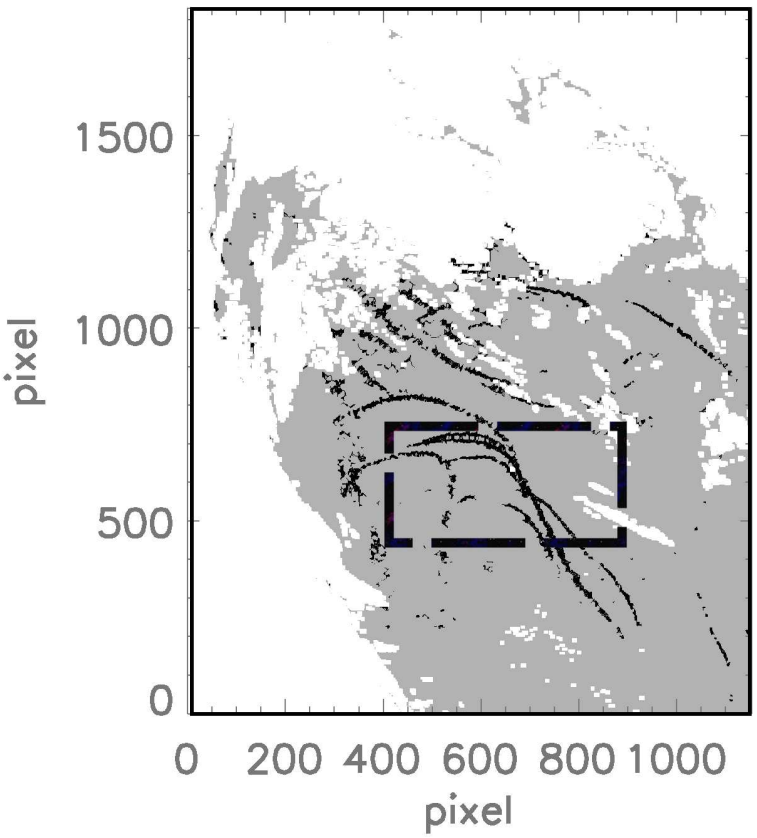

Fig. 10. Result of the ship track mask. Ship-track-pixels are indicated in black and no-track-pixels in grey. Ship-track- and no-track-pixels (grey and black) are low-cloud-pixels. The rectangle shows the smaller selected area.

ACPD
6, 1023–1071, 2006

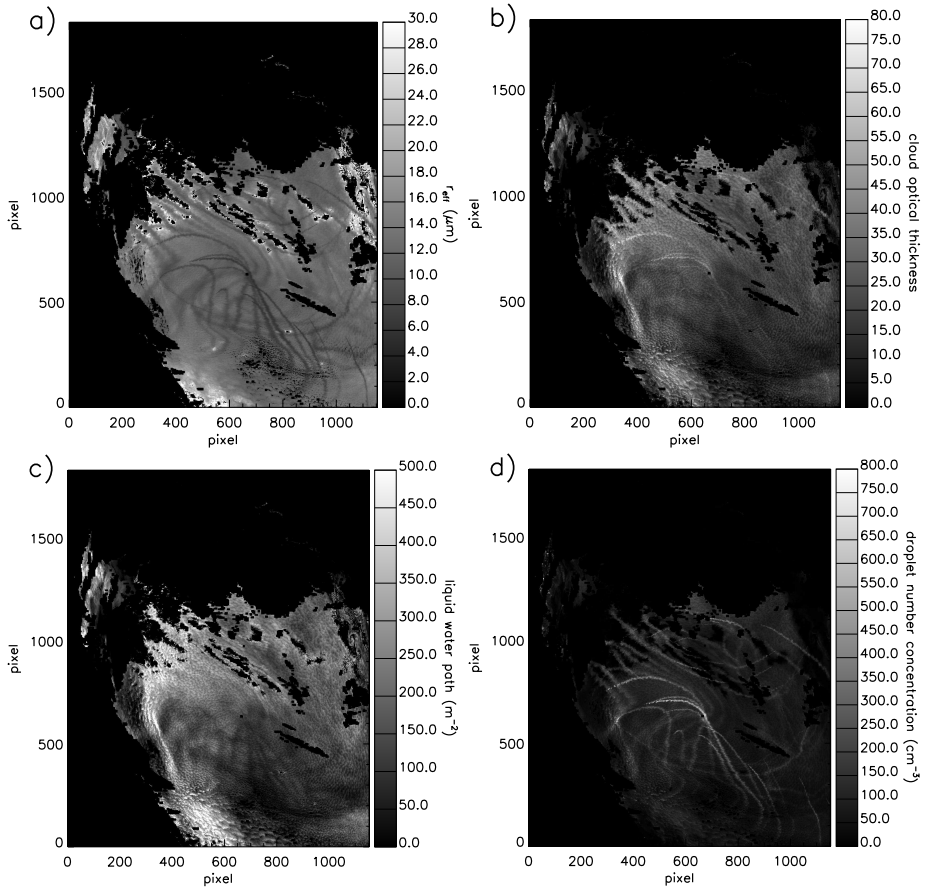

Fig. 11. Effective Radius **(a)**, cloud optical thickness, liquid water path **(c)** and concentration of particles (cm^{-3}) derived from the MODIS channels 2 and 6 for the analysed scene.

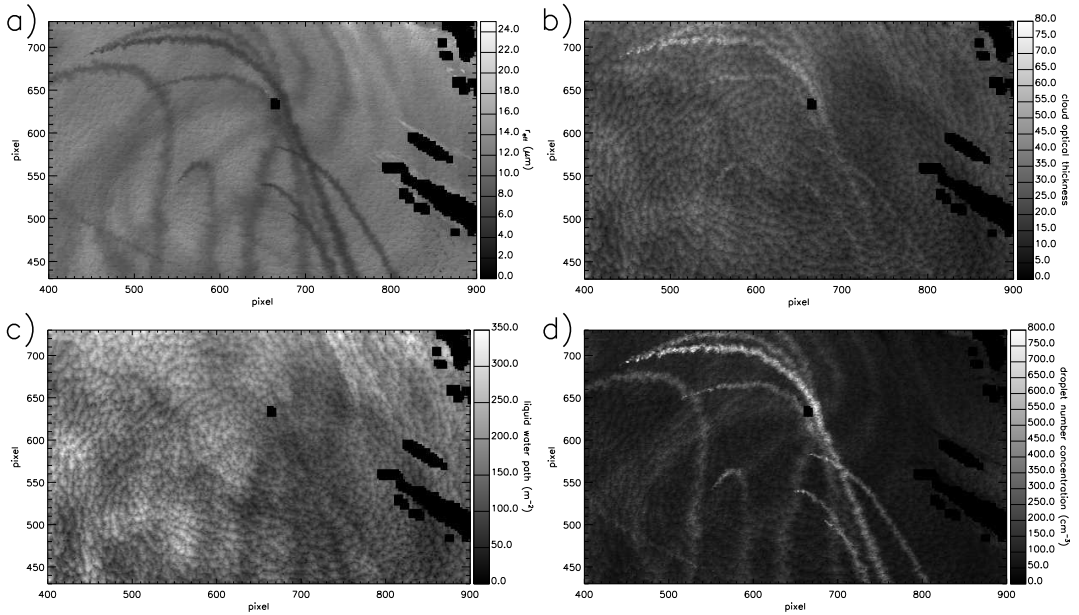

Fig. 12. Effective radius **(a)**, cloud optical thickness **(b)**, liquid water path **(c)** and droplet number concentration **(d)** derived from the MODIS channels 2 and 6 for the smaller selected area.

ACPD
6, 1023–1071, 2006

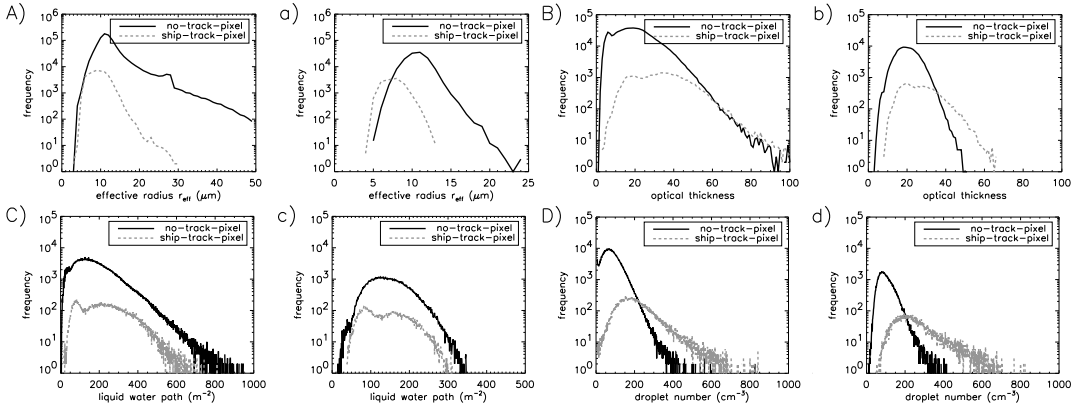

Fig. 13. Statistical distributions of the parameters for the no-track-pixel and the ship-track pixel for the entire scene (capital letters) and the smaller selected scene (lowercase letters): **(A, a)** effective radius, **(B, b)** cloud optical thickness, **(C, c)** liquid water path, **(D, d)** droplet number concentration.

ACPD
6, 1023–1071, 2006

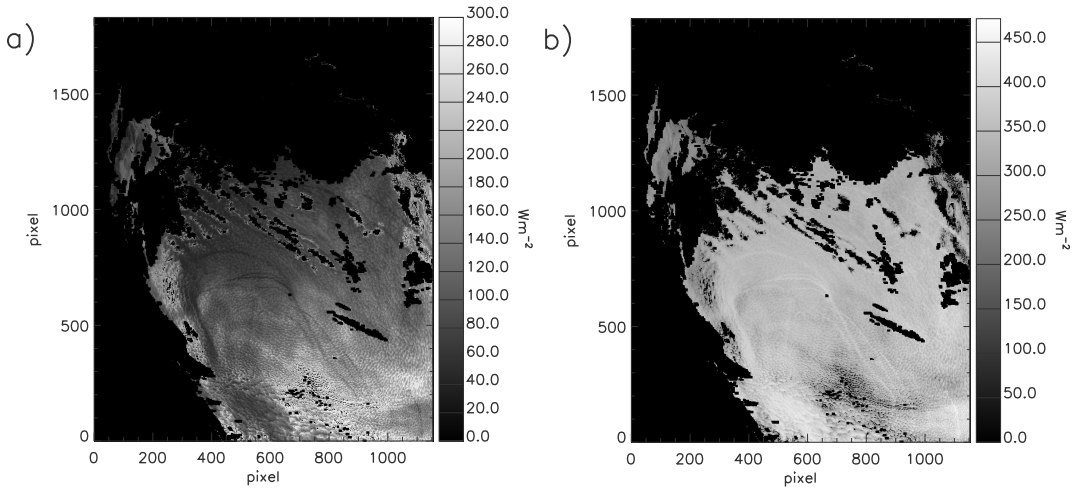

Fig. 14. Down-welling solar radiation at the surface below the clouds (a, in Wm^{-2}) and **(b)** reflected solar radiation on TOA due to the clouds (b, in Wm^{-2}).

ACPD
6, 1023–1071, 2006

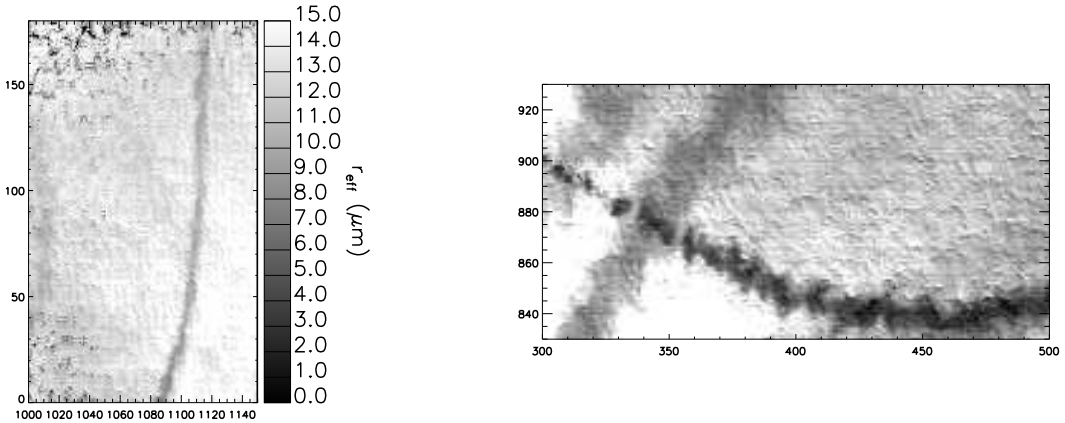

Fig. 15. Possible drizzle suppression areas in the data (r_{eff} in μm).

ACPD

6, 1023–1071, 2006